DEVELOPMENTAL DYNAMICS 235:1100–1106, 2006

TECHNIQUES

Multicolor In Vivo Time-Lapse Imaging at Cellular Resolution by Stereomicroscopy

Martin Distel, Andreas Babaryka, and Reinhard W. Köster*

Intravital time-lapse imaging has altered significantly many long-standing rules of biological mechanisms, but being apparatus-intense and laborious, time-lapse imaging remained mostly restricted to specialized labs. We show that recently introduced fully automated fluorescence stereomicroscopes represent cost-effective but powerful means of imaging dynamic events ranging from observing embryogenesis over several days to detailed tissue rearrangements and fast blood cell rolling in vivo. When combined with deconvolution approaches, even subcellular resolution in several colors can be achieved. Using three-dimensional image recording, we show the spatial reconstruction of expression patterns. Furthermore, by combining three-dimensional image recording over time with subsequent deconvolution analysis, we demonstrate that subcellular dynamics such as axonal pathfinding in vivo can be resolved. These findings promise that time-lapse imaging using a stereomicroscope will become a hands-on standard method for phenotype analysis in many fields of biology. *Developmental Dynamics 235:1100–1106, 2006.*

Key words: zebrafish; bio-imaging; time-lapse; stereomicroscopy; fluorescence

Accepted 22 December 2005

INTRODUCTION

Biological processes such as embryonic morphogenesis, cell migration, wound healing, axon and blood vessel pathfinding are of dynamic nature. Commonly, these processes are being analyzed by static methods with deducing cell and tissue behavior from changes in sets of images recorded at different time points. As informative as such studies have been, they carry the intrinsic danger of missing crucial events or misinterpreting the obtained data (Lichtman and Fraser, 2001). For example, retinal axons lacking the Robo2 receptor often misproject into the ipsilateral area of the tectum, suggesting a role in controlling midline-crossing for this receptor (Fricke et al., 2001). As subsequent time-lapse imaging in zebrafish embryos revealed that wild-type axons occasionally show the same initial misrouting, it became evident that Robo2 confers to an axonal growth cone the ability to prevent or correct misprojections rather than unambiguously selecting its projection trajectory (Hutson and Chien, 2002). This underscores that dynamic cellular events require dynamic analytical methods to be fully understood.

Despite the wealth of data unraveled by time-lapse microscopy, this technique has not become a standard analytical tool for intravital phenotype diagnosis. This finding may be due to the fact that time-lapse microscopy is a time-consuming, laborious, and expertise-demanding analysis requiring lengthy periods of image recording on costly equipment such as confocal microscopes. In contrast, stereomicroscopes can be found in nearly any laboratory and every biologist is familiar with their use. Due to their immense working distance, their high depth of field, and their dual light path generating a three-dimensional image, stereomicroscopes have been the favorite optical setup for the ob-

The Supplementary Material referred to in this article can be found at http://www.interscience.wiley.com/jpages/1058-8388/suppmat

GSF – National Research Center for Environment and Health, Institute of Developmental Genetics, Ingolstädter, Neuherberg-Munich, Germany

Grant sponsor: the German Bundesministerium für Bildung und Forschung; Grant number: Biofuture-Award 0311889.

***Correspondence to: Reinhard W. Köster, GSF – National Research Center for Environment and Health, Institute of Developmental Genetics, Ingolstädter Landstrasse 1, 85764 Neuherberg-Munich, Germany. E-mail: reinhard.koester@gsf.de**

DOI 10.1002/dvdy.20694
Published online 2 February 2006 in Wiley InterScience (www.interscience.wiley.com).

TABLE 1. Comparison of Stereomicroscope and Compound Microscope Objectives[a]

Objective	Numerical aperture	Lateral resolution in μm	Axial-resolution in μm
MZ16FA – Planapo 1.0 zoom 0.71–11.5	0.021–0.141	13.4–2.0	1247.2–27.7
MZ16FA – Planapo 5.0 zoom 0.71–11.5	0.084–0.5	3.3–0.6	77.9–2.2
C Plan 4.0 (Leica)	0.1	2.8	55.0
Plan Neofluar 5.0 (Zeiss)	0.15	1.9	24.4

[a]Numerical apertures (NA) of stereomicroscope objectives with zooming properties are in the similar range or can even surpass the NAs of low-magnification objectives from compound microscopes (data provided by Leica Microsystems). As the lateral resolution ($0.51 \times \lambda_{em}/NA$) and axial resolution ($n \times \lambda_{em}/NA^2$) only depend on the numerical aperture, similar resolutions are achieved with both objectives, making intravital time-lapse microscopy accessible for fully automated fluorescence stereomicroscopes. Examples given here have been calculated with refraction index $n = 1.0$, $\lambda_{em} = 550$ nm.

servation of embryonic or adult laboratory model organisms as well as for specimen and tissue manipulations. Over several decades though, stereomicroscope construction and design has remained essentially unaltered; thus, they mainly remained a dissection tool but had no significant relevance for vital analytical time-lapse recording.

Probably triggered by the discovery and further engineering of increasing numbers of genetically encoded fluorescent proteins over the past years (Chalfie et al., 1994; Matz et al., 1999; Nagai et al., 2002; Shaner et al., 2004; Miyawaki, 2005), stereomicroscopes have experienced an impressive renaissance. Becoming successively equipped with fluorescence excitation, multicolor filter wheels, and even remote focusing controls, the first fully automated stereomicroscope and camera units have been introduced recently. This advancement motivated us to establish intravital three-dimensional long-term time-lapse recording techniques for stereomicroscopes, thereby converting the stereomicroscope from a mainly optical dissecting tool to a powerful but easy to use analytical instrument for observing in vivo dynamics at cellular resolution by still using the stereomicroscope-specific advantages such as the great working distance and high depth of field. This process should render intravital time-lapse imaging into a widely used standard technique for recording cell and tissue dynamics as well as phenotype analysis.

RESULTS AND DISCUSSION

Stereomicroscopes usually are equipped with objectives that provide a great depth of field at the cost of lateral resolution. This finding is due to the low numerical apertures of stereomicroscope objectives. With the development of extensive zooming properties for such objectives, numerical apertures at high magnifications have reached similar or even surpassing values of typical low magnification objectives of compound microscopes. For example, the objectives of the MZ16FA (Leica Microsystems) reach numerical apertures between 0.021 (Planapo 1.0, zoom: 0.71) and 0.5 (Planapo 5.0, zoom: 11.5), whereas numerical apertures of similar ×5 objectives of compound microscopes range around 0.1 (Table 1). Thus, three-dimensional (3D) time-lapse imaging with such recently developed fully automated stereomicroscopes should provide sufficient resolution to follow tissue rearrangements and individual cells within living embryos. Reaching this goal would make time-lapse imaging more amenable to biologists in many fields due to the significantly lower costs of a stereomicroscopic setup compared with confocal microscopes (stereomicroscope setup with 3D deconvolution software ca. 60,000Euro, confocal microscope setup with image rendering software ca. 300,000Euro).

The zebrafish embryo is one of the preferred vertebrate model organisms for bio-imaging approaches due to its transparency, external development, and ease of manipulation. We first established culture conditions to allow long-term image recording. Mounting of the embryos in 1.2% ultra-low gelling agarose was performed as described in detail (Köster and Fraser, 2004). A simple but effective evaporation protection was constructed from two snuggly- fitting, nested but sliding cylinders of polymethylmethacrylate almost sealing the space between the moving objective and the microscope base. In addition, the stereomicroscope was insulated by a chamber fed with air from a low power heater (80Watts, TX7, Lyon Electric Company, Inc.) to provide zebrafish embryos with their physiological temperature of 28°C (Supplementary Fig. S1, which can be viewed at http://www.interscience.wiley.com/jpages/1058-8388/suppmat).

To test the feasibility of this setup, zebrafish embryogenesis was recorded starting right after fertilization with image capturing every 2 or 5 min for periods of up to 3 consecutive days. Not only cell behavior such as the cleavages of the first blastomeres could be followed in detail (Fig. 1a–c), but also cytoplasmic streams (Maegawa et al., 1999) from the yolk into the embryonic cells (Fig. 1b, arrowhead, see Supplementary Movie 1). At subsequent stages, gastrulation movements such as epiboly, axis formation, somitogenesis, and eye and ear development could be observed with the embryo eventually starting to contract somitic muscles and to form pigment (see Supplementary Movie 2).

To capture a distinct morphogenetic process, image recording was focused on the formation of the fourth brain ventricle. This analysis revealed that, between 17 and 19 hr postfertilization

(hpf), the neural rod of the zebrafish hindbrain cavitates along the neuraxis starting from anterior to posterior (Fig. 1d,e, white arrowhead) as has been shown recently with Texas Red dextran injections (Lowery and Sive, 2005). Furthermore, melanocytes become visible at around 26 hpf due to melanin production (Fig. 1f, white arrowhead). Intriguingly, they migrate across the developing cerebellum lining the rhombic lip (Fig. 1g, see Supplementary Movie 3). This finding demonstrates that time-lapse stereomicroscopy is able to reveal the dynamics of morphogenetic processes at cellular resolution.

To increase the resolution of the analysis of hindbrain morphogenetic rearrangements, we switched from a Planapo 1.0 to a Planapo 5.0 objective, resulting in an approximately fivefold increase of the numerical aperture. Instead of capturing a single plane, we recorded z-stacks of images of the hindbrain region over time. Capturing data from three-dimensions rather than from a single plane allows out-of-focus signal to be efficiently eliminated by deconvolution—an iterative mathematical approach based on Fourier-transformations using the point spread function of the microscopic setup (McNally et al., 1999). Starting at 18 hpf, the ventricle formation is clearly visible (Fig. 1h, white star). While the cells at the midbrain–hind-

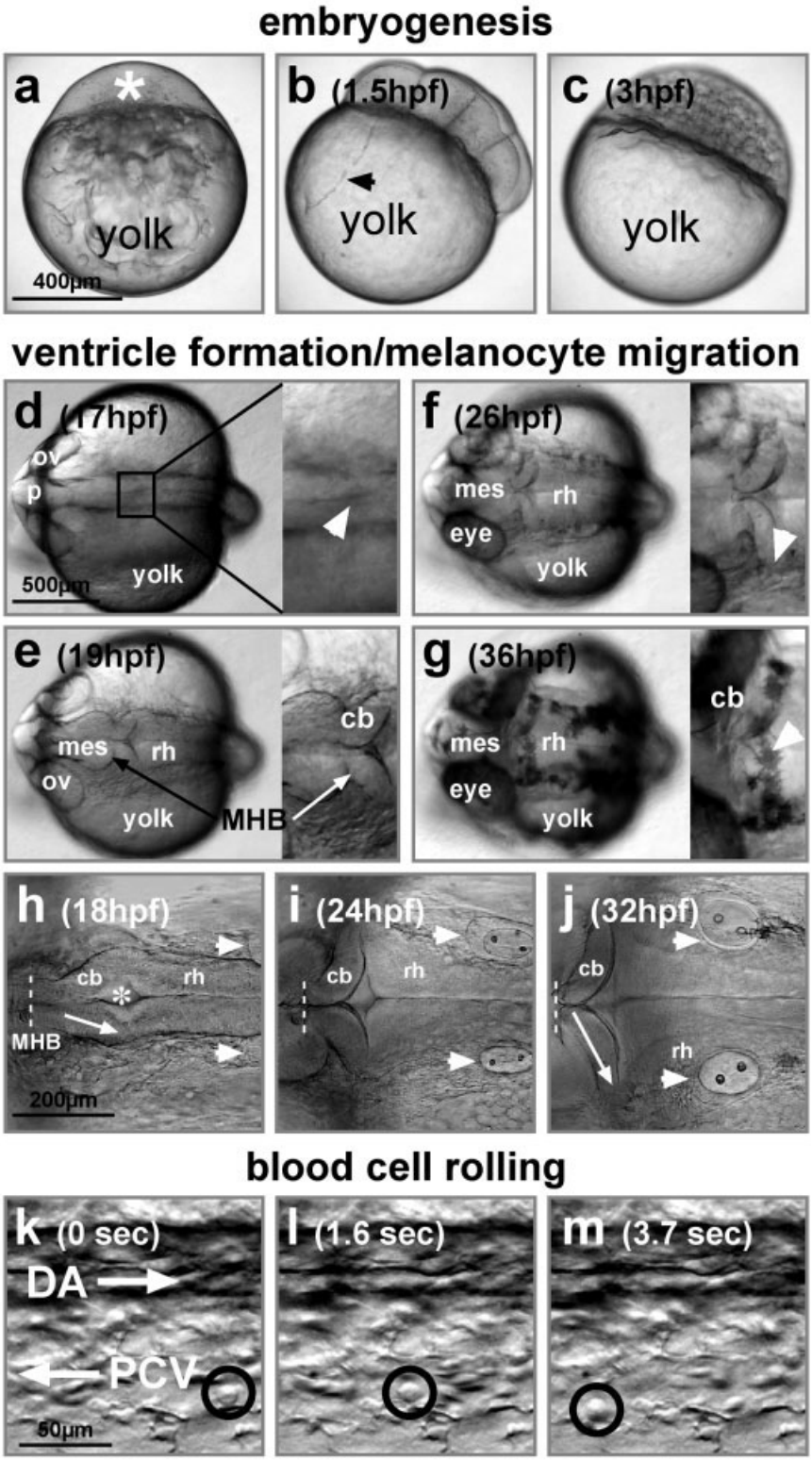

Fig. 1. Bright-field time-lapse stereomicroscopy of zebrafish embryos. **a–c:** Time-lapse analysis displaying morphogenetic changes during zebrafish embryogenesis. First cleavages of blastomeres beginning at the one-cell stage (a, white star) can be followed. Recording conditions: ×1 objective, single plane, every 2 min. See also Supplementary Movie 1 and 2. **d–g:** Time-lapse analysis of fourth ventricle formation in the developing zebrafish hindbrain; digital zoom of cerebellar region is displayed on the right of each picture. Note explorative membrane protrusions of individual melanocytes (f, white arrowhead). Recording conditions: ×1 objective, single plane, every 4 min. See also Supplementary Movie 3. **h–j:** Time-lapse analysis of the rotation of the developing zebrafish cerebellum. Cells at the midbrain–hindbrain boundary (MHB; dashed line) remain together during fourth ventricle opening (white star), leading to a rotation of the cerebellar primordium (compare white arrows in h and j). Note compaction of the hindbrain by shortening of the distance between MHB and otic vesicles (white arrowheads). Recording conditions: ×5 objective, 25 planes at 2 µm distance each, every 12 min for 14 hr, images of individual time points were deconvoluted (settings in Leica Deblur: image spacing 0.997, adaptive PSF, 10 iterations, low noise) and converted in a single sum projection. See also Supplementary Movie 4. **k–m:** Blood cell rolling along the endothelium of the posterior cardinal vein in 32 hours postfertilization (hpf) old embryo; traced cell is marked by black circle. Recoding conditions: ×5 objective, single plane, nearly every 0.1 sec. See also Supplementary Movie 5. cb, cerebellum; DA, dorsal aorta; mes, mesencephalon; ov, optic vesicle; p, prosencephalon; PCV, posterior cardinal vein; rh, rhombencephalon.

brain boundary (MHB; dashed line) remain together, the hindbrain ventricle opens extensively (see Supplementary Movie 4). This change causes the primordium of the cerebellum just posterior to the MHB to rotate around its dorsoventral axis changing from a rostrocaudal to a mediolateral orientation (Fig. 1h,j, compare white arrows). Furthermore, the position of the MHB remains almost unaltered, whereas the otic vesicles (Fig. 1, h–j, white arrowheads) become positioned much closer to the MHB over time (at 18 hpf MHB–otic vesicle distance, 400 μm; at 32 hpf MHB–otic vesicle distance, 250 μm), indicating that the hindbrain condenses significantly during differentiation. Thus, time-lapse stereomicroscopy is able to capture details of morphogenetic tissue rearrangements during embryonic development.

Using the streaming modus of the camera (maximal temporal resolution of 8 frames per second at 512 × 512 pixels), the possible resolution of moderate dynamic processes was tested by recording blood flow in the posterior cardinal vein (PCV) of a 32 hpf embryo. Although delineating erythrocyte movements require faster acquisition speeds (Hove et al., 2003), rolling of individual blood cells along the venous wall could be captured successfully (Fig. 1h–j, black circle; see Supplementary Movie 5). Such behavior is characteristic for blood cell types involved in inflammatory processes such as leukocytes and neutrophils (Kubes and Kerfoot, 2001; Ley, 2002). This finding promises that inflammatory response dynamics can be imaged at the individual cell level directly in vivo (Redd et al., 2004).

While brightfield microscopy resolves the dynamics of tissue compartments or of few individual cell types with intrinsic labeling (such as melanocytes), imaging at the cellular level usually requires specific labeling with fluorescent markers such as dyes or the genetically encoded green fluorescent protein (GFP). To prove the feasibility of automated fluorescence stereomicroscopy for capturing dynamic multicolor information over time, we made use of zebrafish embryos expressing the fluorescent protein Kaede, which can be converted from green to red fluorescence emission by ultraviolet (UV) irradiation (Ando et al., 2002). Kaede-mRNA injection at the one-cell stage resulted in green fluorescent embryos at 10 hpf (Fig. 2a). To record the dynamics of Kaede-conversion, the embryos were exposed to blue (450–490 nm, 60 msec), UV (350–390 nm, 1.5 sec) and green (532–588 nm, 60 msec) light every 30 sec (see Supplementary Movie 6). A rapid decrease in green and concomitant increase in red fluorescence could be observed with the fluorescent protein being almost completely converted after 50 cycles (Fig. 2b). This finding demonstrates the capability of automated fluorescence stereomicroscopes for intravital multicolor time-lapse analysis.

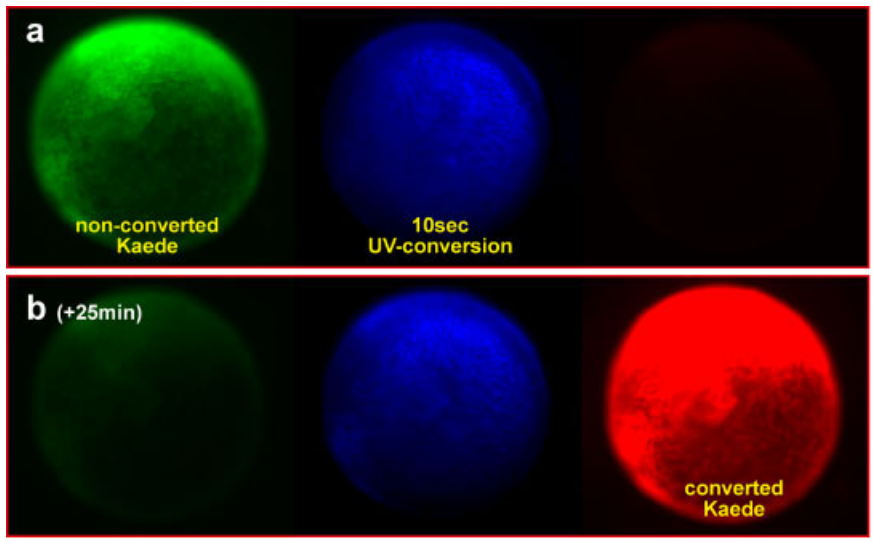

Fig. 2. Multicolor time-lapse recording of fluorescent zebrafish embryo. **a,b:** Time-lapse analysis displaying conversion dynamics of Kaede (MBL International) in zebrafish embryos. Recording conditions: ×1 objective; single plane; filter routine: GFP (60 msec)/DAPI (1.5 sec)/Texas Red (60 msec) every 30 sec, respectively. See also Supplementary Movie 6.

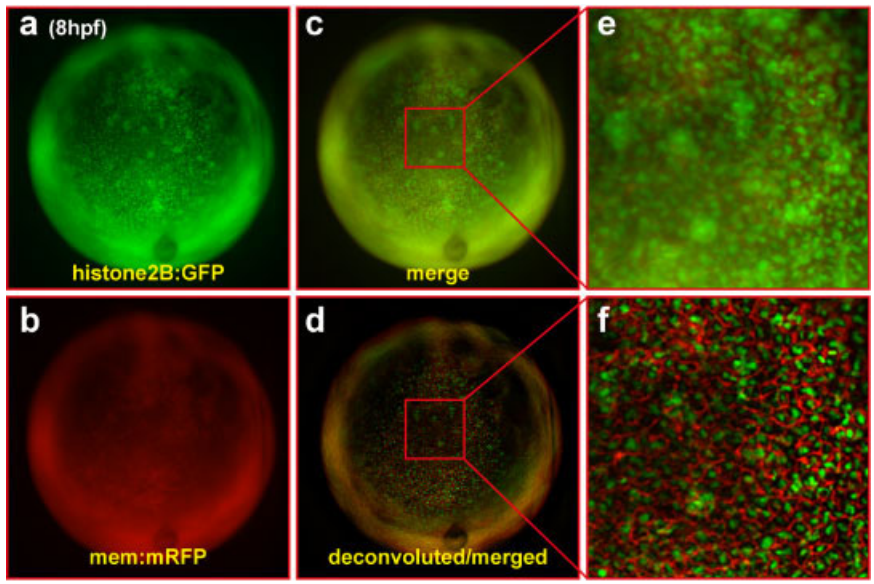

Fig. 3. Subcellular resolution by deconvolution approaches with z-stack recordings of a stereomicroscope. **a,b:** z-stack recording and deconvolution of 8 hours postfertilization (hpf) embryo coexpressing histone2B::GFP (a) and mem::mRFP (b). **c,d:** Merged picture of a single plane from both channels (c) before and (d) after deconvolution. **e,f:** Digital magnifications (ca. 4×) of the animal pole region of the embryos displayed in c and d, respectively. Recording conditions: ×5 objective; z-stack, 128 μm with 2 μm spacing; deconvolution settings in Leica Deblur: image spacing 0.853, adaptive PSF, 10 iterations, low noise.

Nonconfocal fluorescence microscopy bears the difficulty of signal overlap from within and outside the focal plane. Thus, fluorescent emission from embryos coexpressing a nuclear targeted histone2b::GFP variant (Fig. 3a) and a cytoplasmic membrane targeted mem::mRFP variant (Fig. 3b) after mRNA injection appear to overlap (Fig. 3c, a merged image of 3a and 3b, 3e is a digital magnification of cells from the animal pole). To circumvent this problem, we used multicolor z-stack recording for subsequent deconvolution analysis. After image processing, individual cells with differently labeled nuclei and cytoplasmic membranes could be clearly resolved (Fig. 3d, 3f is digital magnification of cells from the animal pole).

When used on transgenic embryos expressing GFP under control of the olig2 enhancer (Shin et al., 2003), z-stack recording with subsequent deconvolution allows even individual axon tracts of motoneurons to be three-dimensionally reconstructed and animated (Fig. 4a,b; see Supplementary Movie 7 for 3D animation). Such detailed but technically simple 3D reconstruction of expression patterns will be very valuable for the analysis of the many GFP transgenic fish strains recently generated by various enhancer trap screens (Grabher et al., 2003; Parinov et al., 2004; Balciunas et al., 2004; Kawakami et al., 2004; Ellingsen et al., 2005).

The astonishing cellular resolution obtained with a stereomicroscope prompted us to ultimately challenge this setup with a dynamic biological problem at the subcellular level: the navigation of axons during embryogenesis. Transgenic olig2:GFP embryos initiate the outgrowth of GFP-expressing secondary motoneuron axons into the somites of the trunk at around 26 hpf. The lateral trunk region of these embryos was imaged under GFP-fluorescence conditions by recording z-stacks of images every 20 min for periods of up to 20 hr. Combining 3D fluorescence time-lapse recording, deconvolution, and image projection allowed individual axons to be followed as they navigated through the somitic tissue. For example, growth cones of axons were found to hold at the myoseptum (Fig. 4c,d, white arrowhead) for more than 3 hr. Here, they project protrusions in several directions before progressing to project further ventrally (Fig. 4e–g), indicating a crucial pathfinding decision at this intermediate target. During later ventral projection, a saltatory progression mode for the growth cone rather than a continuous movement was observed (see Supplementary Movie 7). In addition, this intravital dynamic analysis indicates that axons of the secondary motoneurons unlike retinal axons project almost straight into their target tissue as deviations from their ventral route or corrections of initial misrouting were never observed (n = 4 movies, 24 axons). Although being able to navigate independently, this absence of initial misrouting may be due to the pioneering network laid down by axons of the earlier projecting primary motoneurons (Pike et al., 1992).

To compare the quality of our time-lapse stereomicroscopy to results obtained with a compound microscope, we repeated the same axon pathfinding analysis using a ×5 Plan Neofluar objective at similar magnification, detector resolution, and deconvolution settings. Again, secondary motoneurons halted at the myoseptum for several hours before projecting ventrally in a saltatory manner (Fig. 4h–l; see Supplementary Movie 8). Whereas both approaches were able to record motor axon pathfinding, the images of the steromicroscopy approach appear to be better resolved. This finding can be explained by the higher numerical aperture of the ×5 stereomicroscope objective at high magnifications (see Table 1). Thus, the zooming optics of a stereomicroscope offer the advantage that they can be adjusted more dynamically to processes that are to be imaged.

We have demonstrated by this set of experiments that, with the newly introduced automated fluorescence stereomicroscopes, dynamic in vivo imaging in brightfield and multicolor mode can be achieved at the cellular and even subcellular level in three dimensions over time. Certain limitations of the used setup have to be kept in mind though. Due to the lack of monochromatic light sources, excitation of fluorophores with the mercury lamp of a stereomicroscope is less specific and efficient when compared with laser-mediated excitation with a confocal microscope. Probably, more-powerful photodiodes may solve this issue in the near future (Martin et al., 2005). In addition, a stereomicroscope is usually equipped with a single camera. Thus, when several fluorescent fluorophores are detected simultaneously with dual excitation/emission filters, less-sensitive RGB cameras are required for picture recording. Alternatively, as in this study, more sensitive monochromatic cameras can be used, but they require successive recording of the emission of each fluorophore involving filter changes. As such mechanical changes are time-consuming, the temporal resolution of multicolor recordings with an automated stereomicroscope is low compared with confocal microscopes. Also, we showed that deconvolution approaches could resolve individual cells and larger subcellular structures with a stereomicroscope. Deconvolution requires lengthy periods of calculation; thus, the final imaging results will only be obtained considerably late after image recording and not instantly as with confocal microscopy. Finally, the low magnification and low resolution of stereomicroscope objectives will make recordings of small cellular structures such as microtubule fibers or secretory vesicles difficult.

Nevertheless, as demonstrated here, an automated stereomicroscope combined with 3D deconvolution software represents a cost-effective, easy to handle, intuitive means of intravital time-lapse recording at a convenient working distance. This approach will prove useful for understanding a wealth of biological processes as demonstrated for morphogenetic tissue rearrangements during embryogenesis, melanocyte migration, leukocyte rolling, 3D reconstruction of expression patterns, and axon pathfinding. In addition to the ones shown here, many more processes can likely be included such as lens or otic vesicle invagination, somite formation, fin and limb budding, 3D microangiography, angiogenesis, wound healing, and tumor cell invasion, in both wild-type and mutant animals. As almost every biologist is familiar with handling stereomicroscopes, we hope to have laid the ground for dynamic imaging, leaving its niche, and becoming a widely

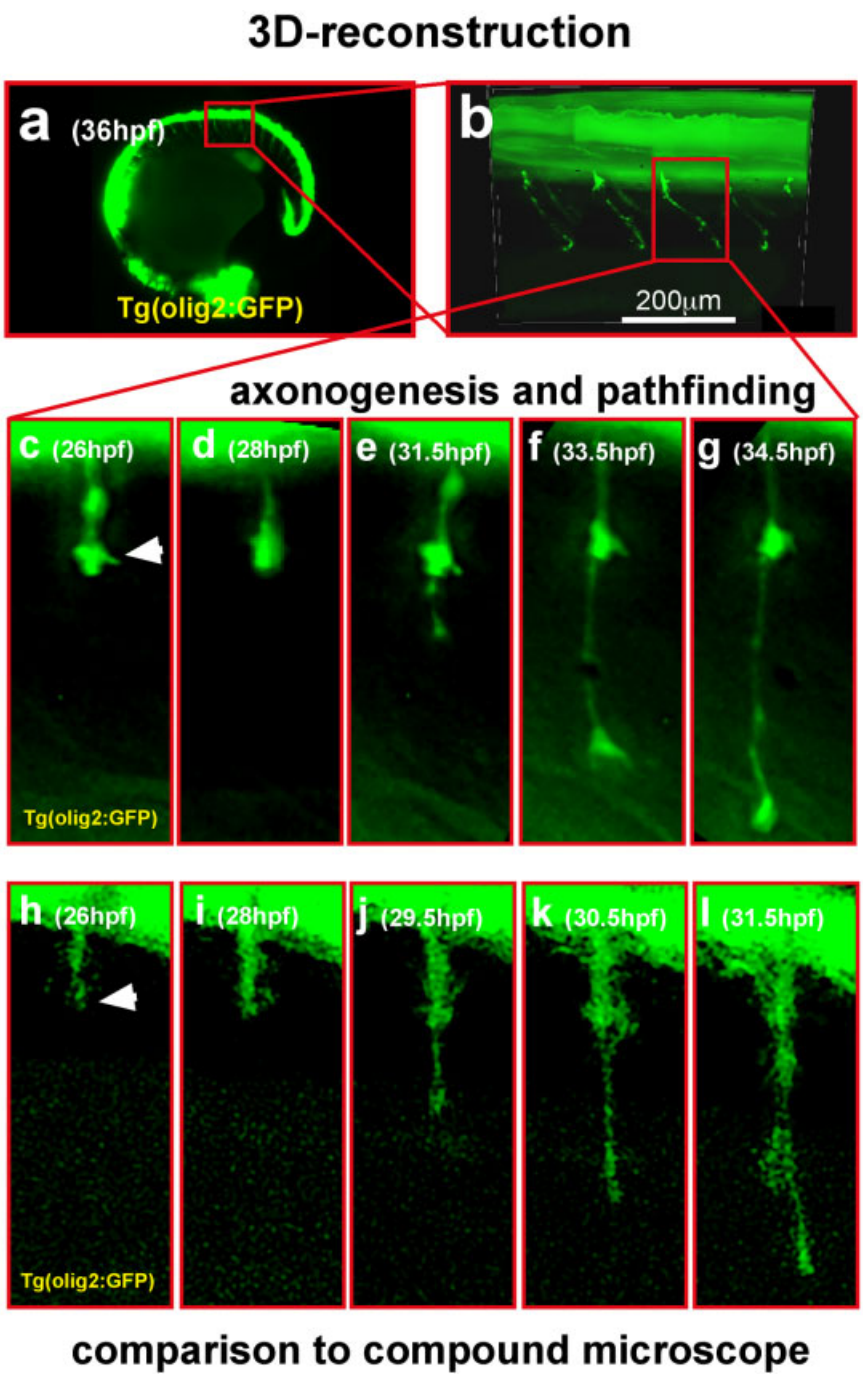

Fig. 4. Three-dimensional (3D) reconstruction of green fluorescent protein (GFP) expression pattern and fluorescence 3D time-lapse stereomicroscopy of motor axon pathfinding in zebrafish embryos. **a,b:** The 3D reconstruction of the trunk region with axons of secondary motoneurons after deconvolution (b) of 36 hours postfertilization (hpf) transgenic olig2:GFP embryo (a). Recording conditions: ×1 objective (a); ×5 objective (b); z-stack, 116 µm with 2 µm spacing; deconvolution settings in Leica Deblur: image spacing 0.226, adaptive PSF, 10 iterations, low noise. **c–g:** The 3D time-lapse recording of axon pathfinding of secondary motoneurons into trunk somites in transgenic olig2:GFP zebrafish embryo using a fluorescence stereomicroscope. Recording conditions: ×5 objective; Planapo NA 0.5; total magnification, ×30; z-stack, 20 µm with 2 µm spacing; deconvoluted images (for settings, see a,b) were subsequently projected into single plane, every 20 min. See also Supplementary Movie 7. **h–l:** The 3D time-lapse recording of axon pathfinding of secondary motoneurons into trunk somites in transgenic olig2:GFP zebrafish embryo using a compound microscope. Recording conditions: ×5 objective; Plan Neofluar NA 0.15, total magnification: ×30, z-stack: 20 µm with 2 µm spacing, deconvoluted images (for settings, see a,b) were subsequently projected into single plane, every 20 min. See also Supplementary Movie 8.

used standard tool for analyzing the dynamics of biological processes in a variety of model organisms, their embryos and adults, in wild-type, mutants, and disease models.

EXPERIMENTAL PROCEDURES

Zebrafish Maintenance

Raising, spawning, and maintaining of zebrafish lines were performed as described (Westerfield, 1995; Kimmel et al., 1995).

Injection

Capped mRNA for microinjection was synthesized from histone2B::EGFP (Kanda et al., 1998), mem::mRFP (Megason and Fraser, 2003), and Kaede (Ando et al., 2002) encoding cDNA cloned in the pCS2+ vector (Rupp et al., 1994) using the SP6 mMESSAGE mMACHINE Kit (Ambion Inc., Austin, TX). Synthesized mRNA was purified with RNeasy spin columns (Qiagen) and subsequent EtOH precipitation. A total of 1.5 nl of 150 ng/µl mRNA solution in 0.05% PhenolRed were injected into the cytoplasm of one-cell stage zebrafish embryos by means of glass capillary tubes.

Imaging

Before image recording, embryos were anesthetized in 0.01% tricaine in 30% Danieau medium containing 0.75 mM phenylthiourea (PTU) to prevent pigmentation. Mounting of embryos in 1.2% ultra-low gelling agarose to restrict embryonic movements was performed as described in detail previously (Köster and Fraser, 2004). As imaging setup, a motorized fluorescence stereomicroscope (MZ16FA, Leica) equipped with a digital camera (DFC350FX, Leica) was used with both being controlled by automating software (FW4000, Leica). For comparison with a compound microscope (Fig. 4), a confocal microscope (LSM510Meta, Zeiss) was used for automated z-stack recording with maximum opening of the pinhole. Deconvolution of the obtained images was performed with the Deblur module of the FW4000 software (Leica). Subsequent image processing, projections, and animations were performed using Photoshop 6.0 (Adobe), After Ef-

fects 6.5 (Adobe), LSM software (Zeiss), and QuickTime 6.5.1 (Apple), respectively.

ACKNOWLEDGMENTS

We thank Christian Leibold and Karl-Heinz Koertje for continuous support. We thank Chichung Lie and Peter Hutzler for critically reading and commenting on the manuscript. We also thank Atsushi Miyawaki for his advice and experimental suggestions. We thank Bruce Appel for providing us with the transgenic olig2:GFP zebrafish line. We thank all members of our laboratory as well as the Wurst, Bally-Cuif, Imai, Graw, and Lie laboratories at the Institute of Developmental Genetics for helpful discussions and suggestions.

REFERENCES

Ando R, Hama H, Yamamoto-Hino M, Mizuno H, Miyawaki A. 2002. An optical marker based on the UV-induced green-to-red photoconversion of a fluorescent protein. Proc Natl Acad Sci U S A 99: 12651–12656.

Balciunas D, Davidson AE, SIvasubbu S, Hermanson SB, Welle Z, Ekker SC. 2004. Enhancer trapping in zebrafish using the Sleeping Beauty transposon. BMC Genomics 5:62.

Chalfie M, Tu Y, Euskirchen G, Ward WW, Prasher DC. 1994. Green fluorescent protein as a marker for gene expression. Science 263:802–805.

Ellingsen S, Laplante MA, König M, Kikuta H, Furmanek T, Hoivik EA, Becker TS. 2005. Large-scale enhancer detection in the zebrafish genome. Development 132:3799–3811.

Fricke C, Lee JS, Geiger-Rudolph S, Bonhoeffer F, Chien CB. 2001. Astray, a zebrafish roundabout homolog required for retinal axon guidance. Science 292:507–510.

Grabher C, Henrich T, Sasado T, Arenz A, Furutani-Seiki M, Wittbrodt J. 2003. Transposon-mediated enhancer trapping in medaka. Gene 322:57–66.

Hove JR, Köster RW, Forouhar AS, Acevedo-Bolton G, Fraser SE, Gharib M. 2003. Intracardiac fluid forces are an essential epigenetic factor for embryonic cardiogenesis. Nature 421:172–177.

Hutson LD, Chien CB. 2002. Pathfinding and error correction by retinal axons: the role of astray/robo2. Neuron 33:205–217.

Kanda T, Sullivan KF, Wahl GM. 1998. Histone-GFP fusion enables sensitive analysis of chromosome dynamics in living mammalian cells. Curr Biol 8:377–385.

Kawakami K, Takeda H, Kawakami N, Kobayashi M, Matsuda N, Mishina M. 2004. A transposon-mediated gene trap approach identifies developmentally regulated genes in zebrafish. Dev Cell 7:133–144.

Kimmel CB, Ballard WW, Kimmel SR, Ullmann B, Schilling TF. 1995. Stages of embryonic development of the zebrafish. Dev Dyn 203:235–310.

Köster RW, Fraser SE. 2004. Time-lapse microscopy of brain development. Methods Cell Biol 76:207–235.

Kubes P, Kerfoot SM. 2001. Leukocyte recruitment in the microcirculation: the roling paradigm revisited. News Physiol Sci 16:76–80.

Ley K. 2002. Integration of inflammatory signals by rolling neutrophils. Immunol Rev 186:8–18.

Lichtman JW, Fraser SE. 2001. The neuronal naturalist: watching neurons in their native habitat. Nat Neurosci 4:1215–1220.

Lowery LA, Sive H. 2005. Initial formation of zebrafish brain ventricles occurs independently of circulation and requires nagie oko and snakehead/atp1a1a.1 gene products. Development 132:2057–2067.

Maegawa S, Yasuda K, Inoue K. 1999. Maternal mRNA localization of zebrafish DAZ-like gene. Mech Dev 81:223–226.

Martin G, Agostini HT, Hansen LL. 2005. Light emitting diode microscope illumination for green fluorescent protein or fluorescein isothiocyanate epifluorescence. Biotechniques 38:204–206.

Matz MV, Fradkov AF, Labas YA, Savitsky AP, Zaraisky AG, Markelov ML, Lukyanov SA. 1999. Fluorescent proteins from nonbioluminescent Anthozoa species. Nat Biotechnol 17:969–973.

McNally JG, Karpova T, Cooper J, Conchello JA. 1999. Three-dimensional imaging by deconvolution microscopy. Methods 19:373–385.

Megason SG, Fraser SE. 2003. Digitizing life at the level of the cell: high-performance laser-scanning microscopy and image analysis for in toto imaging of development. Mech Dev 120:1407–1420.

Miyawaki A. 2005. Innovations in the imaging of brain functions using fluorescent proteins. Neuron 48:189–199.

Nagai T, Ibata K, Park ES, Kubota M, Mikoshiba K, Miyawaki A. 2002. A variant of yellow fluorescent protein with fast and efficient maturation for cell-biological applications. Nat Biotechnol 20:87–90.

Parinov S, Kondrichin I, Korzh V, Emelyanov A. 2004. Tol2 transposon-mediated enhancer trap to identify developmentally regulated zebrafish genes in vivo. Dev Dyn 231:449–459.

Pike SH, Melancon EF, Eisen JS. 1992. Pathfinding by zebrafish motoneurons in the absence of normal pioneer axons. Development 114:825–831.

Redd MJ, Cooper L, Wood W, Stramer B, Martin P. 2004. Wound healing and inflammation: embryos reveal the way to perfect repair. Philos Trans R Soc Lond Series B Biol Sci 359:777–784.

Rupp RAW, Snider L, Weintraub H. 1994. Xenopus embryos regulate the nuclear-localization of Xmyod. Genes Dev 8:1311–1323.

Shaner NC, Campbell RE, Steinbach PA, Giepmans BNG, Palmer AE, Tsien RY. 2004. Improved monomeric red, orange and yellow fluorescent proteins derived from Discosoma sp. red fluorescent protein. Nat Biotechnol 22:1567–1572.

Shin J, Park H-C, Topczewska JM, Mawdsley DJ, Appel B. 2003. Neural cell fate analysis in zebrafish using olig2 BAC transgenics. Methods Cell Sci 25:7–14.

Westerfield M. 1995. The zebrafish book. Eugene, OR: University of Oregon Press.